Effect of Concentration on the Photoinduced Aggregation of Polymer Nanoparticles

Chunlin Zhou,[†] Yue Zhao,[‡] Tze-Chi Jao,[||] Chi Wu,*[,‡,§] and Mitchell A. Winnik*[,†]

Department of Chemistry, University of Toronto, Toronto, Canada, M5S 3H6, The Open Laboratory of Bond-selective Chemistry, Department of Chemical Physics, The University of Science & Technology of China, Hefei, Anhui 230026, China, Department of Chemistry, The Chinese University of Hong Kong, Shatin, N.T. Hong Kong, and Ethyl Petroleum Additives, Inc., 500 Spring St., Richmond, Virginia 23218-2189

Received: January 31, 2002; In Final Form: April 24, 2002

We describe the effect of concentration on the photoinduced flocculation and aggregation of a nonaqueous dispersion of core−shell nanoparticles (diameter = 50 nm), which consist of a tightly cross-linked core composed of poly(butyl methacrylate-*co*-ethylene glycol dimethacrylate) and a lightly cross-linked shell of poly(butyl methacrylate-*co*-ethylene glycol dimethacrylate-*co*-methacrylic acid). The particles could be dispersed in cyclohexane after modification of the acid groups by ester formation with 2-bromo-1-phenyl-octadecan-1-one. Photocleavage of these substituents ($\lambda = 310$ nm) regenerated the −COOH groups and led to aggregation of the destabilized particles. Since the rate of aggregation is relatively slow in this system, we were able to study the process of particle aggregation kinetics by a combination of static and dynamic laser light scattering. Our results indicate, for particle dispersions from 0.23 mg/mL to 0.93 mg/mL, that there are three stages in the aggregation process. Initially, several particles come into contact to form small elongated clusters. Subsequently, these clusters undergo further aggregation to form larger aggregates characterized by a fractal dimension of around 2.3. This result indicates that aggregation in the second stage follows a reaction-limited cluster−cluster aggregation mechanism. At very long times, the aggregate size appears to level off, consistent with a reversible aggregation mechanism. We also found for the three different concentrations that the measured average radius of gyration $\langle R_{g,app} \rangle$ during aggregation scaled with time with an exponent of about 1.4 ± 0.1.

Introduction

We recently described experiments on the photoinduced aggregation of core−shell colloidal particles dispersed in cyclohexane as the continuous medium.[1,2] These particles, with a mean diameter (dry) of 50 nm, have a narrow size distribution and can be dispersed in aliphatic hydrocarbon solvents. The $-C_{16}H_{33}$ chains in the stabilizer are attached to the particle shell by α-benzoyl ester groups. Upon irradiation with UV light ($\lambda = 310$ nm), this group fragments, leaving in its place a much more polar −COOH group. Flocculation is driven by an absence of the stabilization by the long-chain esters and by the tendency of the −COOH groups to dimerize. Since aggregation is very slow in cyclohexane, it provides adequate time to carry out dynamic (DLS) and static (SLS) laser light-scattering measurements as the aggregation process proceeds. Light-scattering measurements provide a direct method to evaluate the fractal dimension d_f of the aggregates, because both the molar mass and the size of the resultant aggregates can be measured directly. In addition, the asymptotic behavior of the scattered intensity $I(q)$ is given by $I(q) \sim q^{-d_f}$ when $R_{aggregate} > q^{-1} > R_{particle}$, where q is the magnitude of the scattering vector. We obtained the same value $d_f \approx 2.3$ from both of types of experiments.

Particle aggregation has been studied both theoretically[3−7] and experimentally[8−13] over the past two decades. It is generally accepted that there exist two limiting regimes for aggregation, diffusion-limited cluster−cluster aggregation (DLCA) and reaction-limited cluster−cluster aggregation (RLCA).[3,4,14−19] These studies have focused on the two fundamental aspects of the aggregation process: the structure of the aggregates and their size evolution. Our understanding of the growth of these ramified structures has benefited from the application of concepts from modern statistical mechanics such as universality, scaling, and fractals.[20] The fractal dimension for aggregates refers to the scaling relationship between their mass (M) and their size (R), $M \sim R^{d_f}$.[4,19,21]

RLCA is observed when there is a barrier to aggregation and when the magnitude of this barrier E_a is larger than kT. Under these conditions, the sticking probability per collision, $p \sim \exp(-E_a/kT)$, is appreciably smaller than unity. A large number of collisions are required before two particles can stick together. This process leads to aggregates with a more compact structure (with d_f in the range 2.0−2.5) than those formed by a diffusion-limited mechanism, because an approaching particle has a higher chance to penetrate into the "fjords" of a cluster before it sticks to the cluster.[5,22,23] In addition, colliding clusters can interpenetrate more if the sticking probability is close to zero. Ball et al.[24] pointed out that in a real experiment, the polydispersity of the resultant clusters could result in a slightly higher value of d_f than that predicted theoretically. Weitz et al.[17] suggested that in the RLCA process, R should increase exponentially with time as $R \sim \exp(At)$, where A is a constant, whose value depends on the system studied.

Almost all of the examples of cluster aggregation described in the literature result from studies carried out in aqueous solution. In these experiments, aggregation was induced by adding salt to the medium, screening the repulsion between electrostatically stabilized colloidal particles. We have a much

* Author to whom correspondence should be addressed.
[†] University of Toronto.
[‡] The University of Science & Technology of China.
[§] The Chinese University of Hong Kong.
[||] Ethyl Petroleum Additives, Inc.

10.1021/jp020306n CCC: $22.00
Published on Web 08/23/2002

poorer understanding of nonaqueous systems where electrostatic effects are much less important. One such system has been described by Bezot et al.,[25] who examined the aggregation of soot particles taken from the oil of diesel truck engines. From the fractal nature of the growing aggregates and the magnitude of the fractal exponent (2.15 ± 0.1), they concluded that these soot particles grow by an RLCA process. The repulsive potential in nonaqueous systems is steric in origin, In our system,[1,2,26] we use a photochemical reaction to decrease the magnitude of the steric barrier, and thereby induce flocculation in the system. We describe how aggregation in this system depends on particle concentration.

Experimental Section

Sample Preparation and Photoreaction. The photolabile core−shell nanoparticles were prepared by a three-step procedure, described in more detail in ref 2. The core is about 20 nm in diameter and consists of a copolymer of butyl methacrylate (BMA) and ethylene glycol dimethacrylate (EGDMA, 4:3 mole ratio). The 13.5 nm thick shell is a copolymer containing BMA (83 mol %), methacrylic acid (MAA, 10 mol %), hydroxyethyl methacrylate (HEMA, 3 mol %), and EGDMA (4 mol %). Half of the carboxylic acid groups were converted to 1-phenyl-1-oxo-2-octadecyl ester chains to help disperse the particles in hydrocarbon solvents. In this experiment, dispersions at four different concentrations (0.10, 0.23, 0.58, and 0.93 mg/mL) were prepared in cyclohexane and then filtered into the light-scattering cell through a 0.45 μm Millipore filter to remove dust. The aggregation of these particles was induced in-situ inside the light-scattering cell by photoirradiation at 310 nm in a photochemical reactor for 4 h. The samples were then transferred to the light-scattering instrument. The photoreactor[1] was homemade, consisting of a box which holds eight 310 nm 15 W lamps (Gu Cun photoelectron factory, Shanghai, China) arranged in two layers on the inside wall of the reactor. Individual samples were suspended by a fine copper wire through the hole in the top of the reactor, and positioned at the level of the bottom layer of lamps. The samples were irradiated directly in the Pyrex light-scattering cell (SUPERLCO 7.4 mL vial, Cat. No. 27150-U).

Laser Light Scattering. Light-scattering measurements were carried out with a modified commercial light-scattering instrument (ALV GmbH, Langen, Germany), equipped with a multi-τ digital time correlator (ALV-5000) and a solid-state laser (ADLAS DPY 425II, output power ca. 400 mW at $\lambda = 532$ nm). The details of this instrument can be found elsewhere.[27] In static LLS, the angular dependence of the absolute excess time-averaged scattered intensity, the Rayleigh ratio, $R_{vv}(q)$, is related to the weight-average molar mass ($M_{w,app}$), the z-average root-mean-square radius of gyration ($\langle R_{g,app}{}^2\rangle_z^{1/2} \equiv \langle R_{g,app}\rangle$) of the scattering objects and the second virial coefficient (A_2) of the dispersion by

$$\frac{Kc}{R_{vv}(\theta)} = \frac{1}{M_{w,app}\left(1 - \frac{1}{3}\langle R_{g,app}{}^2\rangle q^2\right)} + 2A_2c \qquad (1)$$

$$\left(\frac{Kc}{R_{vv}(\theta)}\right)^{1/2} = \left(\frac{1}{M_{w,app}\left(1 - \frac{1}{6}\langle R_{g,app}{}^2\rangle q^2\right)} + 2A_2c\right)^{1/2} \qquad (2)$$

where K is a constant for a given dispersion, temperature and laser, and q [$= (4\pi n/\lambda)\sin(\theta/2)$] is the scattering vector with n, λ, and θ being the refractive index of solvent, the wavelength of the light in a vacuum, and the scattering angle, respectively.

CHART 1

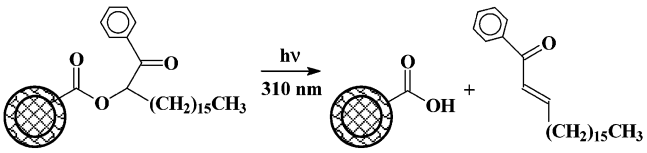

Values of $M_{w,app}$ and $\langle R_{g,app}\rangle$ were calculated in two ways. In the Zimm method (eq 1), the ALV software fits the values $Kc/R_{vv}(q)$ vs q^2 to a line, and then calculates the intercept at $q = 0$ to obtain $M_{w,app}$ and the slope to obtain $\langle R_{g,app}\rangle$. In the Berry method (eq 2), it fits $(Kc/R_{vv}(q))^{1/2}$ vs q^2 to a polynomial of order 4, and calculates $M_{w,app}$ and $\langle R_{g,app}\rangle$ from the intercept and tangent at the intercept, respectively. In this research, the size of the aggregates grows from 40 nm to approximately 500 nm. To analyze the data for this wide range of aggregate sizes, we used the Zimm method[28] to calculate $\langle R_{g,app}\rangle$ and $M_{w,app}$ when the rms radius of gyration $\langle R_{g,app}\rangle$ was less than 100 nm, and the Berry method[29] when $\langle R_{g,app}\rangle$ was larger than 100 nm. For conditions in which $\langle R_{g,app}\rangle \leq 100$ nm, both methods gave identical values of $M_{w,app}$ and $\langle R_{g,app}\rangle$. For larger objects, eq 1 often led to negative values of $M_{w,app}$.

For a fractal object formed by aggregation of colloidal particles, the scattered intensity $I(q)$ scales with q as $I(q) \sim q^{-d_f}$ in the range of $R_{aggregate} > q^{-1} > R_{particle}$, where d_f is the fractal dimension. $R_{particle}$ and $R_{aggregate}$ are the radii of the primary particles and the resultant aggregate, respectively.[30] When $q^{-1} < R_{particle}$, the light probes the internal structure of the primary particles and the intensity profile reflects the density distribution inside, whereas when $q^{-1} > R_{aggregate}$, the experiment is sensitive to the overall size of the aggregates.

In dynamic light scattering (DLS), the cumulant analysis of the measured intensity−intensity time correlation function $G^{(2)}(q,t)$ in the self-beating mode provides an average line-width ($\langle\Gamma\rangle$), and Laplace inversion analysis provides the line-width distribution ($G(\Gamma)$).[31,32] For a pure diffusive relaxation, Γ can be related to the translational diffusion coefficient D via $\Gamma = Dq^2$ in the limit of $c \rightarrow 0$ and $q \rightarrow 0$,[33] where c is the concentration of scatterers. The hydrodynamic radius ($R_{h,app}$) can be calculated by the Stokes−Einstein equation

$$D = k_BT/(6\pi\eta R_{h,app}) \qquad (3)$$

where k_B is the Boltzmann constant, T is the absolute temperature, and η is the solvent viscosity. Therefore, $G(\Gamma)$ can be converted to a hydrodynamic radius distribution $f(R_{h,app})$: From each line width distribution $G(\Gamma)$ or hydrodynamic radius distribution $f(R_{h,app})$, we calculate an average line width ($\langle\Gamma\rangle$, defined as $\int_0^\infty G(\Gamma)\Gamma\, d\Gamma$) or an average hydrodynamic radius ($\langle R_{h,app}\rangle$, defined as $\int_0^\infty f(R_{h,app})R_{h,app}\, dR_{h,app}$) characteristic of the sample. The variation of the size distribution as a function of time can be better viewed by examining the relative width of the distribution [$(\mu_2/\langle\Gamma\rangle^2)$ of $G(\Gamma)$], where μ_2 is defined as $\int_0^\infty G(\Gamma)(\Gamma - \langle\Gamma\rangle)^2\, d\Gamma$.

Results and Discussion

In this paper, we consider the influence of particle concentration on the photoinduced flocculation of sterically stabilized core−shell particles dispersed in cyclohexane. The photochemical reaction that leads to flocculation is depicted in Chart 1. Ester cleavage replaces the nonpolar $C_{16}H_{33}$ ester groups with more polar carboxylic acid groups. Our most reliable information about the influence of the photochemical reaction on the dimensions of individual particles comes from the most dilute sample, at a concentration of 0.10 mg/mL. This sample,

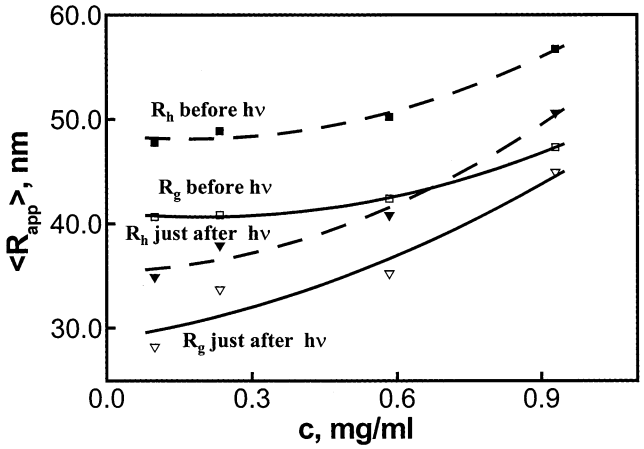

Figure 1. Concentration dependence of the average size ($\langle R_{app} \rangle$) of PBMA core−shell nanoparticles. UV light ($\lambda = 310$ nm) was used to cleave the stabilizing α-benzoyl heptadecyl chains.

remarkably, does not undergo any detectable aggregation. The particles when dry have a diameter of 50 nm. Dispersed in cyclohexane, the particles swell. The diameter measured by DLS is 95 nm. The swelling is largely confined to the lightly cross-linked shell (dry thickness 13 nm), since the core of the particle is highly cross-linked. Cleavage of the ester groups leads to deswelling of the shell. After irradiation, the hydrodynamic diameter of the particle drops to 80 nm. It is important to note that the C_{16} chains have a fully stretched length of only ca. 2 nm, whereas both $\langle R_{h,app} \rangle$ and $\langle R_{g,app} \rangle$ decrease by about 7 nm. This result can be understood by recognizing that removal of the ester groups and their conversion into −COOH groups will decrease the quality of the solvent for the polymer in this shell. In other words, the photoreaction increases the magnitude of the Flory−Huggins χ parameter for the shell polymer in cyclohexane, accompanied by a deswelling of this shell.

In Figure 1 we plot the apparent values of the average hydrodynamic radius $\langle R_{h,app} \rangle$ and the average radius of gyration $\langle R_{g,app} \rangle$ of the particles in cyclohexane, before and after photoirradiation, as a function the concentration of the core−shell nanoparticles. The values of $\langle R_{h,app} \rangle$ are essentially identical at 0.10 and 0.23 mg/mL, whereas the values of $\langle R_{g,app} \rangle$ increase with increasing particle concentration. These values are stable over short periods of time, prior to the onset of flocculation. We find that both values increase with concentration, before and just after UV irradiation. Under these conditions, the ratio of $\langle R_{g,app} \rangle / \langle R_{h,app} \rangle$ remains almost constant and close to the theoretical value of 0.78 predicted for uniform spheres. After irradiation, the particles at 0.23, 0.58, and 0.93 mg/mL flocculate to form aggregates over time. The increase in aggregate size can be monitored by light scattering. When flocculation begins, it is likely driven by a combination of two effects. Contraction of the shell leads to a stronger van der Waals attraction between particles. In addition, deswelling of the shell reduces the repulsive interaction due to osmotic and steric effects between the shells of adjacent particles.

Evolution of the Size and Structure of the Aggregates. In Figure 2a we plot the measured values of the average number of particles ($M_{w,app}/M_0$) as a function of time. One sees first that the time scale for the particle growth process ranges from 50 h for the most concentrated dispersion to nearly 200 h for the sample at 0.23 mg/mL. These times are much longer than the 4 h needed for complete photoreaction.[34] Aggregation is sufficiently slow that we could measure the angular dependence of the integrated (static) light-scattering intensity as a function of aggregation time. These are the data needed to calculate the

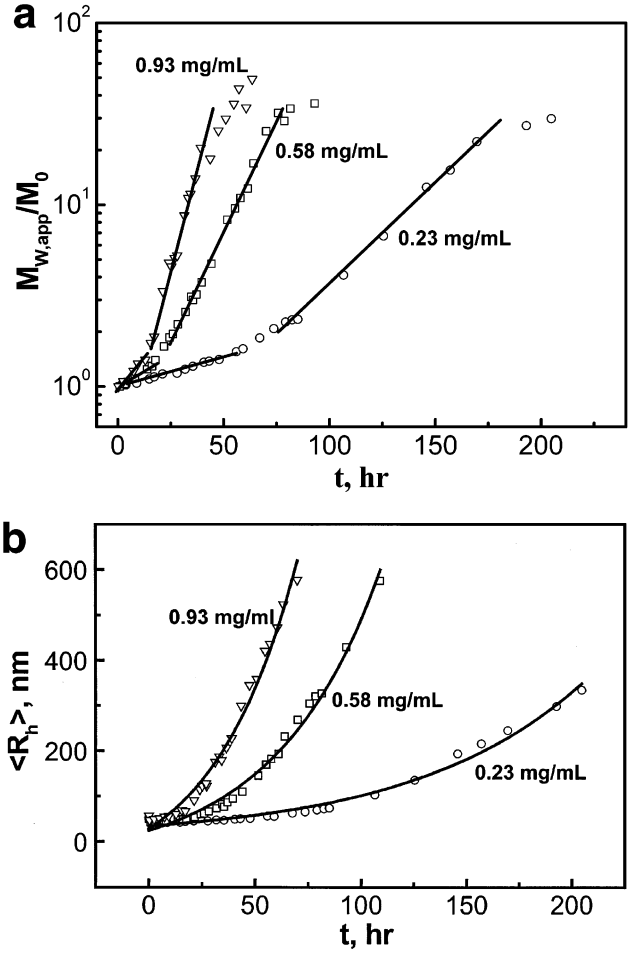

Figure 2. Time dependence, for the three different particle concentrations, of (a) the average number of particles per aggregate ($M_{w,app}/M_0$), and (b) the average hydrodynamic radius of the aggregates $\langle R_{h,app} \rangle$.

weight-averaged molecular weight of the aggregates as a function of time, as well as their radius of gyration $\langle R_{g,app} \rangle$. The data in Figure 2 suggest that the growth of the aggregates occurs in two stages, an initial slow step to form dimers, trimers, and other small aggregates, followed by a more rapid process that leads to aggregates containing up to 150 primary particles. There is also a suggestion in the data that particle size levels off at long times. This could occur only if aggregation were reversible and the dissociation step dominated as the aggregate size increased.

In Figure 2b we examine the influence of concentration on the rate of growth of the hydrodynamic radius of the aggregates. Even for the highest particle concentration, there is little growth over the first 10 h after the photochemical step was complete. We find that all the data exhibit an exponential dependence of $\langle R_{h,app} \rangle$ on aggregation time. The slow rate of the aggregation process suggests that the aggregation is reaction controlled rather than diffusion limited. The curves in Figure 2b can be fitted to the expressions

$$\langle R_{h,app} \rangle \text{ (nm)} = -1.26 + 32.4 \exp(0.0116t) \quad \text{for 0.23 mg/mL} \quad (4a)$$

$$\langle R_{h,app} \rangle \text{ (nm)} = -67.8 + 83.9 \exp(0.0190t) \quad \text{for 0.58 mg/mL} \quad (4b)$$

$$\langle R_{h,app} \rangle \text{ (nm)} = -12.9 + 146 \exp(0.0233t) \quad \text{for 0.93 mg/mL} \quad (4c)$$

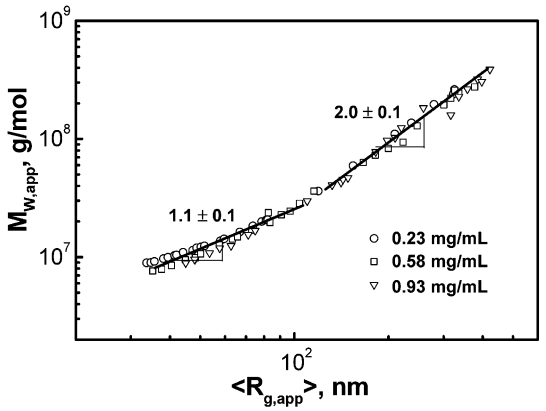

Figure 3. Scaling relationship between the weight average molar mass ($M_{w,app}$) and the *z*-average apparent radius of gyration ($\langle R_{g,app}\rangle$) for the aggregates formed at three different primary particle concentrations.

The negative intercepts point to problems with the fit at early times. This result is consistent with an early stage component to the particle growth process that is not properly accommodated by a simple exponential growth expression. The time evolution of $\langle R_{g,app}\rangle$ also supports the idea of two stages in the particle growth mechanism. In a log−log plot (see Supporting Information), we find a long induction period, especially at low particle concentration, followed by a strong increase in the rate of aggregate growth. If the late-stage data are fitted to a power law, the mean radius of gyration scales with time with an exponent of 1.4 ± 0.1. This value is higher than predicted and measured for the RLCA mechanism,[35,36] but consistent with results that we have reported previously for this system. [1]

In Figure 3 we plot the increase in $M_{w,app}$ against the corresponding increase in the average radius of gyration $\langle R_{g,app}\rangle$. These data also show two stages in the aggregation process, with a crossover occurring at $\langle R_{g,app}\rangle \approx 120$ nm. In the first stage, all of the data fit the relationship $M_{w,app} \sim \langle R_{g,app}\rangle^{1.1+0.1}$. On close inspection, it appears that there is a slightly higher power-law exponent for the sample at the highest concentration, but the major conclusion is that for all three concentrations, all of the data fall on a common line. This regime is characterized by small aggregates, containing up to about 6 to 8 primary particles. From the magnitude of the power-law exponent, we deduce that these small aggregates are elongated in shape rather than compact. After the crossover, all the data collapse together and the scaling exponent increases to 2.0 ± 0.1, a value characteristic of fractal aggregates formed through an RLCA process.

Consistent with this idea is that the density of the aggregates decreases with increasing size. The density of the aggregates is calculated according to $\rho = M_{w,app}/[(4\pi/3)\langle R_{h,app}\rangle^3 N_A]$, where N_A is Avogadro's number. In plots of log ρ vs log $\langle R_{h,app}\rangle$, all the data fit a common line with a slope of −1.3 ± 0.1. This result is typical of open aggregates whose void volume is filled with solvent. Further evidence for the fractal structure of these large aggregates is provided by the *q*-dependence of the scattering intensity. At late stages of the aggregation, it is possible to carry out experiments in the range of $\langle R_{g,app}\rangle > q^{-1}$. All the data (see Supporting Information) fit a power-law dependence, with $I(q) \sim q^{-2.3}$ for the low concentration (0.23 mg/mL) dispersion and $I(q) \sim q^{-2.4}$ for the two higher concentration dispersions (0.58 and 0.93 mg/mL). These values are slightly higher than the power-law exponent obtained from the log $M_{w,app}$ vs log $\langle R_{g,app}\rangle$ plot. The magnitude of the scaling exponents, however, is consistent with aggregates formed in a reaction-limited cluster aggregation process.

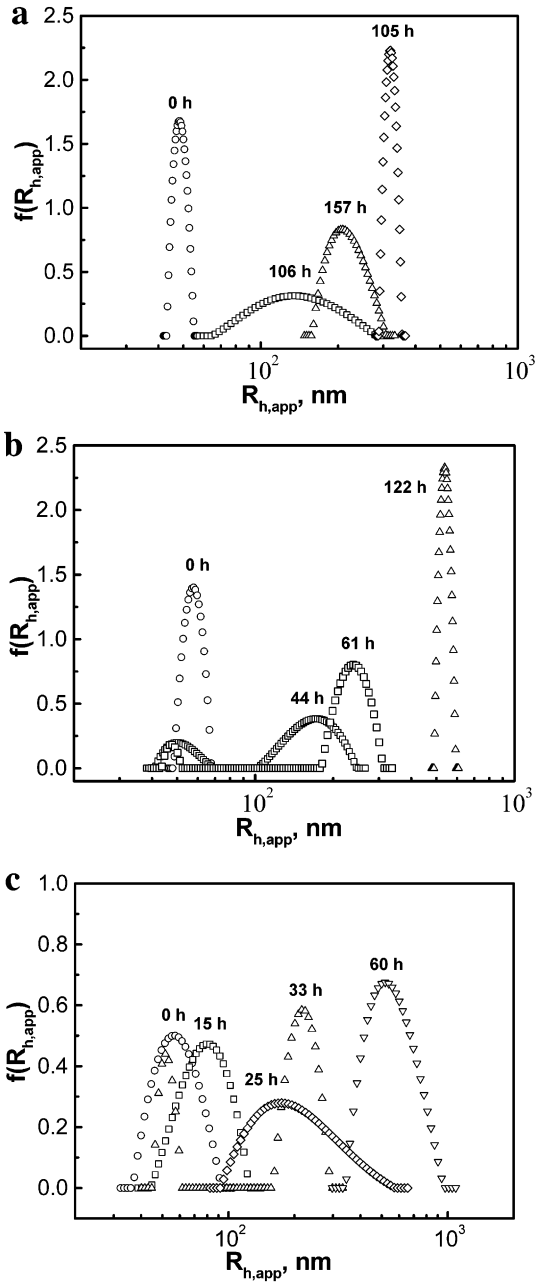

Figure 4. Time dependence of the hydrodynamic radius distribution ($f(R_{h,app})$) of the aggregates formed at primary particle concentrations of (a) 0.23 mg/mL, (b) 0.58 mg/mL, and (c) 0.93 mg/mL.

Evolution of the Size Distribution. The particles we examine, prior to irradiation, have a very narrow size distribution. As aggregation proceeds, one expects the size distribution to broaden. There are two common measures of size distribution that one can obtain from DLS experiments. From Laplace inversion, one can calculate the hydrodynamic radius distribution $f(R_{h,app})$ from the line width distribution, and one can calculate the second cumulant $\mu_2/\langle\Gamma\rangle^2$ from a cumulant expansion of the dynamic light-scattering signal. In Figure 4 we plot the change in hydrodynamic radius distribution $f(R_{h,app})$ against $R_{h,app}$ for samples at different concentrations following photoirradiation for similar times. The plot at zero time shows that the original particles after irradiation have a narrow size distribution, which is somewhat broader for the sample at the highest particle concentration. In the initial stages of aggregation, the size distribution broadens, and the peak is shifted to a larger radius.

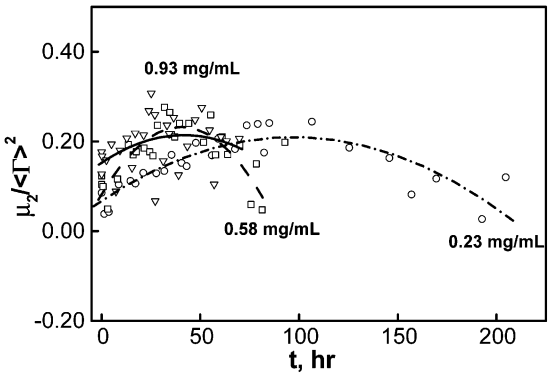

Figure 5. Time dependence of the relative width ($\mu_2/\langle\Gamma\rangle^2$) of the linewidth distribution ($G(\Gamma)$) for the aggregates formed at three different primary particle concentrations, where $\mu_2 = \int_0^\infty G(\Gamma)(\Gamma - \langle\Gamma\rangle)^2\, d\Gamma$and $\langle\Gamma\rangle = \int_0^\infty G(\Gamma)\, \Gamma\, d\Gamma$.

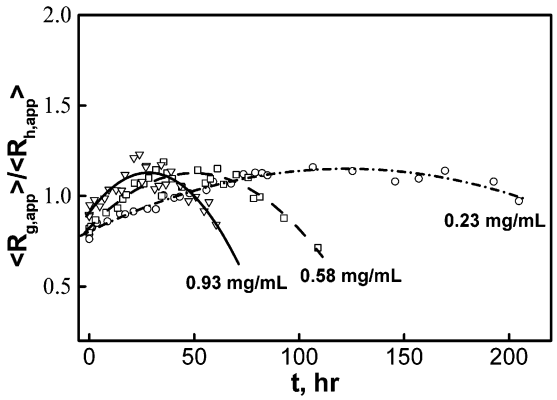

Figure 6. Time dependence of the ratio of the apparent radius of gyration to the apparent hydrodynamic radius for aggregates formed at three different primary particle concentrations.

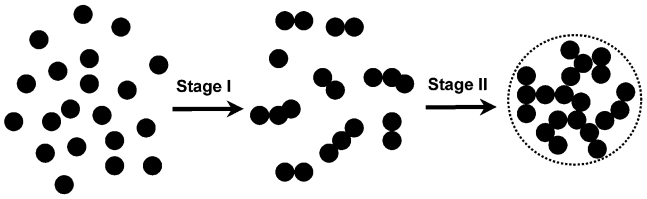

Figure 7. Schematic representation of the two stages of aggregation following UV irradiation.

Later stages of aggregation lead to larger aggregates, but with a much narrower size distribution.

This type of evolution of the size distribution is unusual. A more common observation in RLCA processes is that the cluster size grows without limit, with the breadth of the distribution increasing throughout the growth process.[36] Because this feature of the growth process was unexpected, we describe it in detail. Examples of the evolution of the distribution for 0.58 and 0.93 mg/mL are presented in Figure 4b,c. At all three concentrations we see that there is a growth in the breadth of the distribution corresponding to the early stage in particle growth in which small, elongated aggregates are formed. At later times the distribution narrows. At higher particle concentrations, the process is faster. For the sample at 0.58 mg/mL, at 44 and 61 h of aggregate growth, we observe a bimodal size distribution (Figure 4b). We also see a bimodal distribution in Figure 4c for the sample after 33 h. These times are close to the crossover in the particle growth mechanism. The peaks at smaller $\langle R_{h,app}\rangle$ correspond to the small aggregates formed in the first stage of cluster growth, whereas the peak at larger $\langle R_{h,app}\rangle$ are likely due to the larger aggregates formed in the second stage. We infer from the bimodal distribution that the crossover between the first and second growth stages does not occur simultaneously throughout the solution. Rather it occurs more gradually and becomes more important once the small aggregates reach a certain size.

In Figure 5, where we plot $\mu_2/\langle\Gamma\rangle^2$ vs time. Here too we see that the initial stages of aggregation led to the formation of clusters with a broad size distribution, and that at later stages, the larger aggregates had a much narrower size distribution. Despite the scatter in the data points, the trend is clear for all there dispersions. For the low concentration dispersion (0.23 mg/mL), the width of the distribution grows over the first 100 h after the photoreaction and then decreases with increasing time. For the higher concentration dispersions (0.58 and 0.93 mg/mL), the growth in the size distribution takes less time, around 30 h, and the subsequent decrease is also faster. These results suggest that aggregation occurs in two stages with very different properties.

Another view of the change in the nature of the aggregates size distribution is provided by the ratio of radius of gyration to hydrodynamic radius ($\langle R_{g,app}\rangle/\langle R_{h,app}\rangle$). As one sees in Figure 6, the initial ratio is close to the value (0.78) predicted for uniform nondraining spheres. As the aggregation proceeds, this ratio increases, suggesting that the shape of the resultant clusters in the first stage is elongated. In the second stage $\langle R_{g,app}\rangle/\langle R_{h,app}\rangle$ decreases, suggesting that at longer times, the aggregation of these elongated small clusters leads to more compact sphere-like structures. The rise and decay of this ratio occurs on a much faster time scale for the sample at the highest particle concentration (0.93 mg/mL) than for the sample at 0.23 mg/mL. The $\langle R_{g,app}\rangle/\langle R_{h,app}\rangle$ ratio for the sample at 0.58 mg/mL evolves on an intermediate time scale.

We summarize our ideas about the two stages of the aggregation process in Figure 7. In the first stage, individual particles stick together to form a mixture of dimers, trimers, and other small clusters, leading to a large increase in the polydispersity of cluster sizes present in the sample. This is the polydispersity one sees in Figure 5 for the samples after the photoreaction. In the second stage, cluster−cluster aggregation becomes dominant, leading to the formation of large aggregates. The aggregation of these small clusters may act like an averaging process, so that the polydispersity decreases.

Another factor is also important. We have some independent evidence that the cluster aggregation in this system is reversible. For example, we have found that if the system is heated to 65 °C, it rapidly deaggregates back to primary particles. We defer to a separate paper that includes a description of the cluster dissociation process. For the purposes of this paper, we use this result to suggest that fragmentation of the clusters may play a role in the experiments described here in limiting the size of the aggregates formed and in narrowing the size of the large aggregates that form at long times.

Kinetics of Cluster Growth. In Figure 2a we saw that cluster size increased exponentially with time, both in the first stage and in the second stage of particle growth, where k_{sh} represents the apparent first-order rate coefficient at short times, and k_l describes the rate at long times.

$$M_{w,app}/M_o = A_{sh} \exp(k_{sh}t) + A_l \exp(k_l t) \qquad (5)$$

The later stage in particular exhibits growth kinetics reminiscent of that ($M \approx A \exp(kt)$) reported by Lin et al.[37] for the salt-induced RLCA aggregation of colloidal gold and silica. We also

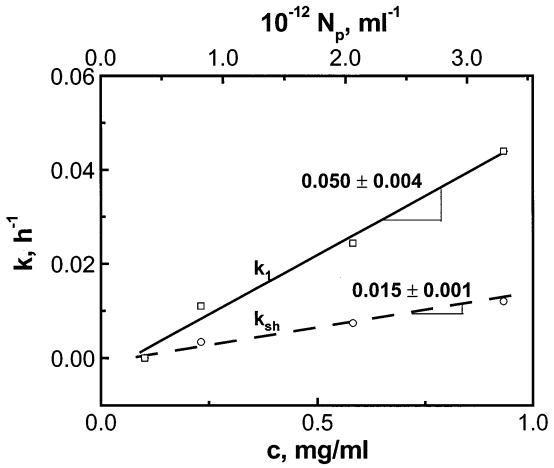

Figure 8. Concentration dependence of the apparent first-order rate constant k during the aggregation of particles following UV irradiation.

TABLE 1: Number of Particles, Rate of Particle Association, and Aggregation Rate Constant for the Core−Shell Particles in Cyclohexane at Four Different Concentrations

c (g/L)	0.10	0.23	0.58	0.93
$c \times 10^{-10}$ (mol/L)	5.9	14	34	55
$N_p \times 10^{-14}$ (1/L)	3.6	8.2	21	33
$-(dc/dt)_d \times 10^9$ (mol L^{-1} s^{-1})	1.3	6.8	43	110
t_d (s) [a]	0.46	0.20	0.079	0.049
k_{sh} (1/h)	0	0.0032	0.0074	0.013
k_1 (1/h)	0	0.011	0.024	0.10

[a] The mean time for two particles at each concentration to diffuse to form a contact pair.

see in Figure 2a that the rate of particle growth increases significantly with the increase in particle concentration.

We examine these results in more detail in Figure 8. We plot the particle concentration dependence of the rate coefficients k_{sh} and k_l, calculated from slopes of the semilog plots in Figure 2a. The lower x-axis describes the particle concentration in g/mL. The top scale describes the number of primary particles per unit volume. We calculate the number density of the primary particles according to equation $N_p = c/[\rho_p(4/3)\pi\langle R_{h,app}\rangle^3]$, where c is the dispersion concentration and ρ_p the density of each particle, here, taken as the density of PBMA (1.05 g/mL) since the main component is PBMA. The results of calculation are listed in Table 1. There are two interesting features of this plot. First we see that both plots are linear. From a kinetic point of view, the system exhibits pseudo-first-order kinetics at each fixed concentration of primary particles. One sees that these pseudo-first-order rate coefficients depend linearly on the particle concentration, a result typical of second-order kinetics. Both plots extrapolate close to the origin, and to values close to zero at the concentration (0.10 mg/mL) of our lowest particle concentration. At this lowest concentration, no particle aggregation can be observed by light scattering.

We have argued that the cluster growth that we observe is characteristic of a reaction-limited aggregation process. In this section we compare the rates we measure to the rate predicated for diffusion-controlled interaction of pairs of primary particles in the initial stage of aggregation. We develop our arguments in terms of the encounter-pair model[38−40] in which a two-particle reaction in a condensed phase consists of two steps: (a) diffusion of the particles together to a fixed encounter radius to form an encounter pair, and (b) subsequent chemical reaction within this encounter pair. The encounter pairs are assumed to be sufficiently long-lived that they can be treated as an equilibrium ensemble. Equation 6 relates the experimental second-order rate constant k to the corresponding rate constant k_{diff} for the diffusion-controlled process and k_{chem} for the reaction-controlled process.

$$\frac{1}{k} = \frac{1}{k_{diff}} + \frac{1}{k_{chem}} \tag{6}$$

Eq 6 takes the limiting value of complete diffusion control ($k = k_{diff}$) if the reaction step is fast, and complete chemical control ($k = k_{chem}$) if the reaction step is slow.

We can estimate the time necessary for the aggregation of two single particles in a diffusion-limited process. If Brownian flocculation is fast and diffusion controlled, as described by Smoluchowski, and sedimentation is assumed to be negligible, the diffusion-controlled rate constant is given by

$$k_{diff} = 8\pi N_A \langle R_{h,app}\rangle D \tag{7}$$

where N_A is Avogadro's number and D is the particle diffusion coefficient. The two-particle association rate for two identical particles is described by second-order kinetics

$$-dc/dt = k_{diff}c^2 \tag{8}$$

where c is the concentration of particles at time t.

The experiments reported here were carried out at particle concentrations of 0.10, 0.23, 0.58, and 0.93 mg/mL, corresponding to 3.6×10^{14}, 8.2×10^{14}, 20.6×10^{14}, and 33.0×10^{14} particles L^{-1}, respectively. To make a connection with the units used to describe diffusion-controlled chemical reactions, we can express these primary particle concentrations as 5.9×10^{-10}, 14×10^{-10}, 34×10^{-10}, and 55×10^{-10} mol/L, respectively.[41]

From the measured values of D and $\langle R_{h,app}\rangle$ we calculate a value of $k_{diff} = 3.7 \times 10^9$ L mol^{-1} s^{-1}. Thus the initial rate of the particle dimerization $[-(dc/dt)_d]$ is estimated to be 1.3×10^{-9}, 6.8×10^{-9}, 4.3×10^{-8}, and 1.1×10^{-7} mol L^{-1} s^{-1}, and the primary particles will diffuse together to form binary contact pairs in 0.46, 0.20, 0.079, and 0.049 s, respectively. With the increase of concentration, the time necessary to form a contact pair decreases. These times are still orders of magnitude smaller than those found in our experiments. Thus we conclude that the aggregation process is reaction limited, even at the highest concentrations that we examined.

Implications for Particle Aggregation in Motor Oil. Our sponsors are interested in these experiments as a model for aggregation processes that occur in motor oil. In automobile engines, condensation products of incomplete fuel consumption leads to sludge formation. In diesel engines, soot is a major contaminant. The experiments of Bezot et al.[25] show that diesel soot forms fractal aggregates by an RLCA mechanism, and are characterized by a fractal exponent of 2.15 ± 0.1. Soot aggregates form from primary particles that have been characterized by electron microscopy. Their size ranges from 20 to 40 nm and is not very sensitive to the source of the soot.[42] Typical soot contains 97% carbon, with the balance of oxygen and sulfur.[43] Its chemical makeup resembles diamond-like carbon,[44] except that diamond-like carbons contain varying amounts of hydrogen instead of oxygen and sulfur. The mixed carbon-bonding character of a given diamond-like carbon form defines the carbon valence-electron density, which is directly related to the carbon density, and thus, the hardness of the carbon material. Jao et al.[42] have used the plasmon energy obtained from low-loss EELS to measure the density of carbon valence

electrons in a variety of diesel soot samples. These were found to be similar in structure with hardness values estimated to range from 830 to 1330 kg/mm^2, sufficiently hard to scratch the metal components of a diesel engine.

The model system that we describe here consists of polymer particles, with a dry diameter of 50 nm, consisting of a glassy, highly cross-linked core surrounded by a soft, solvent-swollen shell. We explain the colloidal stability of our particles before photo-irradiation in terms of a combination of two effects: osmotic and entropic stabilization from the loops and chain ends protruding from the lightly cross-linked particle shell, coupled with a relatively weak van der Waals attraction between the particles when the shell is strongly swollen by solvent. Following the photocleavage reaction, there is a decrease in the extent swelling of the shell, resulting in an increase in the van der Waals attraction and a decrease in steric stabilization. For this system in cyclohexane, aggregation occurs on a time scale of tens of hours and is sensitive to the particle concentration. In other alkane solvents, such as octane and cyclohexane−hexadecane mixtures, which are much poorer solvents for the lightly cross-linked shell polymer, flocculation is substantially faster. Here precipitation can be observed on a time scale of minutes to tens of minutes.

The question that strikes us in the context of our experiments is why the aggregation of soot particles studied by Bezot et al. is so slow. These authors took soot samples from used diesel oil which contained 4 wt % soot, diluted them in base oil (viscosity 18 cP at 40 °C) to ca. 10^{-5} g/mL, and subjected the mixture to 1 h ultrasonic shearing. They followed aggregation by a combination of static and dynamic light scattering at 40 °C over a period of 200 h, during which aggregates grew from about 20 primary particles to more than 3000. We note that their experiments were carried out at a particle concentration 10-fold lower than our experiments described above, and their solvent was approximately 20-fold more viscous. Both factors will slow the aggregation rate relative to the conditions we employed.

If small soot aggregates present after the sonication step had bare surfaces, it would be difficult to explain reaction-limited aggregation. The van der Waals attraction between pairs of dense carbon particles is significantly stronger than that between polymer particles with a solvent-swollen shell. Without an activation barrier to flocculation, aggregation should occur by a diffusion-limited process. While the origin of the barrier to diesel soot aggregation is unknown, it may be due to adsorption of polymeric additives present in the oil.[45]

Summary

We used a combination of static and dynamic laser light scattering to investigate the concentration-dependence of flocculation of polymer particles in cyclohexane at 25 °C. The particles have a core−shell structure, with a tightly cross-linked core and a lightly cross-linked shell. Flocculation is induced photochemically through a reaction that converts nonpolar ester groups in the shell to more polar carboxylic acid groups.

Aggregate growth occurs in a two-step process. In the first step, primary particles associate to form small, elongated structures with a broad size distribution. In the second stage, these small structures undergo further aggregation to form larger structures, with a relatively narrow size distribution, containing up to 150 primary particles. These structures are characterized by a fractal exponent of 2.3. There is no evidence for precipitation or sedimentation of these clusters at very long times. In fact, these clusters appear to reach a maximum size, which leads us to infer that aggregation is a reversible process. We note that when a solution containing large aggregates is heated to 65 °C, the aggregates dissociate back to primary particles. This dissociation process will be the subject of a future publication.[46]

The cluster growth process is very slow in cyclohexane, requiring more than 150 h at a concentration of 0.23 mg/mL. The growth rate is faster at elevated particle concentration, occurring over 70 h at 0.58 mg/mL and 40 h at 0.93 mg/mL. Both the first stage and the second stage of the aggregation process follow overall first-order kinetics, with first-order rate coefficients that depend linearly on particle concentration. Thus these rate coefficients behave like pseudo-first-order rate constants in an overall second-order process. This type of behavior seems too simple to describe a system involving the aggregation of intermediates of different sizes. Another curious observation is that the sample at the lowest particle concentration, 0.010 mg/mL, does not aggregate at all on the time scale of these experiments.

Cluster growth in this system depends on a delicate balance of the attractive and repulsive forces between primary particles. In the initial dispersed state, the particle shell is strongly swollen by the cyclohexane solvent. The repulsive osmotic and steric forces dominate the van der Waals attraction between particles. Following the photochemical reaction, the shell shrinks in dimensions, although it is still swollen compared to the dry particle dimensions. The repulsive forces decrease in magnitude and are accompanied by an increase in the attractive forces. The net interaction is attractive, and likely not so strong as to lead to irreversible bonding between adjacent particles within an aggregate.

Acknowledgment. The financial support of the RGC of HKSAR Earmarked Grant 1998/99 (CUHK 4209/99P, 2160122), the CAS Bai Ren Project, Ethyl Petroleum Additives, Inc., and NSERC Canada is gratefully acknowledged.

Supporting Information Available: Additional figures showing plots of log $\langle R_{g,app} \rangle$ vs log time, plots of log I vs log q, and log(density) vs log $\langle R_{h,app} \rangle$ are provided. This material is available free of charge via the Internet at http://pubs.acs.org.

References and Notes

(1) Zhou, C.; Zhao, Y.; Jao, T. C.; Winnik, M. A.; Wu, C. *J. Phys. Chem. B* **2002**, *106*, 1889.
(2) Zhou, C.; Winnik, M. A.; Jao, T. C. *J. Polym. Sci., Part A: Polym. Chem.* **2001**, *39*, 2642.
(3) Witten, T. A., Jr.; Sander, L. M. *Phys. Rev. Lett.* **1981**, *47*, 1400.
(4) Meakin, P. *Phys. Rev. Lett.* **1983**, *51*, 1119.
(5) Brown, W. D.; Ball, R. C. *J. Phys. A* **1985**, *18*, L517.
(6) Martin, J. E.; Ackerson, B. J. *Phys. Rev. A* **1985**, *31*, 1180.
(7) Jullien, R.; Botet, R.; Mors, P. M. *Faraday Discuss. Chem. Soc.* **1987**, *83*, 125.
(8) Schaefer, D. W.; Martin, J. E.; Wiltzius, P.; Cannell, D. S. *Phys. Rev. Lett.* **1984**, *52*, 2371.
(9) Aubert, C.; Cannell, D. S. *Phys. Rev. Lett.* **1986**, *56*, 738.
(10) Lin, M. Y.; Lindsay, H. M.; Weitz, D. A.; Ball, R. C.; Klein, R.; Meakin, P. *Nature* **1989**, *339*, 360.
(11) Zhou, Z.; Chu, B. *J. Colloid Interface Sci.* **1991**, *143*, 356.
(12) Burns, J. L.; Yan, Y.; Jameson, G. J.; Biggs, S. *Langmuir* **1997**, *13*, 6413.
(13) Zhu, P. W.; Napper, D. H. *Phys. Rev. E* **1994**, *50*, 1360; *Colloids Surf. A* **1995**, *98*, 93.
(14) Kolb, M.; Botet, R.; Jullien, R. *Phys. Rev. Lett.* **1983**, *51*, 1123.
(15) Jullien, R.; Kolb, M. *J. Phys. A* **1984**, *17*, L771.
(16) Von Schulthess, G. K.; Benedek, G. B.; Deblois, R. W. *Macromolecules* **1980**, *13*, 939.
(17) Weitz, D. A.; Huang, J. S.; Lin, M. Y.; Sung, J. *Phys. Rev. Lett.* **1985**, *54*, 1416.

(18) Lin, M. Y.; Lindsay, H. M.; Weitz, D. A.; Ball, R. C.; Klein, R.; Meakin, P. *Phys. Rev. A* **1990**, *41*, 2005.
(19) Reinecke, H.; Mijangos, C.; Lopez, D.; Guenet, J. *Macromolecules* **2000**, *33*, 2049.
(20) Family, F.; Landau, D. P. *Kinetics of Aggregation and Gelation*, Elsevier: Amsterdam, 1984.
(21) Wiltzius, P. *Phys. Rev. Lett.* **1987**, *58*, 710.
(22) Peng, S.; Wu, C. *Macromolecules* **1999**, *32*, 585.
(23) (a) Vicsek, T. *Fractal Growth Phenomena*; World Scientific: London, 1992. (b) Halsey, T. C. *Phys. Today* **2000**, *11*, 36.
(24) Ball, R. C.; Weitz, D. A.; Written, T. A.; Leyvraz, F. *Phys. Rev. Lett.* **1987**, *58*, 274.
(25) Bezot, P.; Hesse-Bezot, C.; Diraison, C. *Carbon* **1997**, *35*, 53.
(26) Liu, Z.; Winnik, M. A.; Jao, T. C.; Rösch, J. *J. Phys. Chem. A* **1998**, *102*, 5349.
(27) Wu, C.; Xia, K. Q. *Rev. Sci. Instrum*. **1994**, *65*, 587.
(28) Zimm, B. H. *J. Chem. Phys.* **1948**, *16*, 1099.
(29) Berry, G. C. *J. Chem. Phys*. **1966**, *44*, 4550.
(30) Kim, A. Y.; Berg, J. C. *Langmuir* **2000**, *16*, 2101.
(31) Berne, B. J.; Pecora, R. *Dynamic Light Scattering*; Plenum Press: New York, 1976.
(32) Chu, B. *Laser Light Scattering*, 2nd ed.; Academic Press: New York, 1991.
(33) Stockmayer, W. H.; Schmidt, M. *Pure Appl. Chem*. **1982**, *54*, 407.
(34) With a better reactor and a quartz cell, the reaction time can be reduced to less than 10 min.
(35) Spirito M. D.; Chiappini, R.; Bassi, F. A.; Stasio E. D.; Giardina, B.; Arcovito, A. *Physica A* **2002**, *304*, 211.
(36) (a) Martin, J. E. *Phys. Rev. A* **1987**, *36*, 3415. (b) Meakin, P. *Adv. Colloid Interface Sci*. **1988**, *28*, 249.
(37) Lin, M. Y.; Lindsay, H. M.; Weitz, D. A.; Ball, R. C.; Klein, R.; Meakin, P. *Proc. R. Soc. London* **1989**, *A 423*, 71.
(38) North, A. M. *Quart. Rev.* **1966**, *20*, 421.
(39) Noyes, R. M. In *Effects of Diffusion Rates on Chemical Kinetics*; Porter, G., Ed.; Pergamon: London, 1961; p 129.
(40) Gilbert, R. G. *Emulsion Polymerization*; Academic Press: London, 1995; p 25.
(41) We use molar concentrations for particles and rate constants to facilitate comparison with reactions between molecules. Physicists prefer number densities. In these units, $k_{diff} = 6.2 \times 10^{-15}$ L s^{-1}.
(42) Jao, T.-C.; Li, S.; Yatsunami, K.; Chen, S. J.; Csontos, A. A.; Howe, J. M. Proceedings of the International Tribology Conference, Nagasaki, Japan,. Japan Society of Tribologists, 2000; Vol. 3, pp 1981−1986.
(43) Bardasz, E. A.; Carrick, V. A.; Ebeling, V. L.; George, H. F.; Graf, M. M.; Kornbrekke, R. E.; Pocinki, S. B. SAE, Paper No. 961915 (1996).
(44) Robertson, J. In *Diamond and Diamond-Like Films and Coatings*; Calusing, R. E., et al., Eds.; Plenum Press: New York, 1991; pp 331−356.
(45) Soot has polar groups at its surface. These are the target for polymeric dispersants added to motor oil to minimize or suppress soot aggregation. Li, S.; Passut, C. A.; Devlin, M. T.; Jao, T.-C. Proceeding of the 5th World Surfactant Congress, Firenze, Italy, May 2000, pp 955−964. In this reference and in ref 25, the authors compared the aggregation rate for samples with and without polymeric additives. These additives slowed the rate of soot aggregation.
(46) Zhou, C.; Li, H.; Zhao, Y.; Wu, C.; Jao, T. C.; Winnik, M. A. Manuscript in preparation.